Reduction by Oxidation: Selective Hydrodehalogenation of Aryl Halides by Mediated Oxalate Oxidation

Joshua A. Beeler[1], Rune P. Walkingshaw[1], Safiya A.S. Hamud[1], Henry S. White[1*]

Affiliations

[1] Department of Chemistry, University of Utah, Salt Lake City, Utah 84112, United States

*Corresponding author: white@chem.utah.edu

Abstract

Electroorganic reduction reactions are canonically carried out at a cathode at which a significant negative potential is applied. Specifically, aryl bromides and chlorides undergo heterogeneous reduction in organic solvents at potentials more negative than –2 V vs $E^{0'}$ for the Fc/Fc$^+$ couple (Fc = ferrocene). To decrease the overpotential for reduction reactions, electrocatalysis strategies are often employed. Here, we present an electrochemical method to *reduce* aryl bromides and chlorides that is initiated by an *oxidation reaction* at very mild potentials (~ 0 V vs Fc/Fc$^+$). Specifically, electrochemical oxidation of an outer-sphere redox mediator, 1,1-dimethylferrocene, in dry *N,N*-dimethylformamide (DMF) containing oxalate ($C_2O_4^{2-}$), results in the homogeneous one-electron oxidation of $C_2O_4^{2-}$. The resulting $C_2O_4^{\bullet-}$ decomposes in ~1 μs to release the carbon dioxide radical anion ($CO_2^{\bullet-}$), a potent reductant that is oxidized to CO_2 at –2.68 V vs Fc/Fc$^+$. In this way, an oxidation reaction at very low electrode potentials enables the homogeneous reduction of aryl bromides and chlorides, which are otherwise directly reduced at very negative potentials. Using this method, selective hydrodehalogenations of electron-deficient aryl bromides and chlorides are carried out at a reticulated vitreous carbon anode with up to quantitative conversion yields. Cyclic voltammetry and finite difference simulations are used to characterize the hydrodehalogenation of 4-bromobenzonitrile via $C_2O_4^{2-}$ oxidation. Additionally, we show that the efficiency of hydrodehalogenation can be tuned by deliberate additions of water to the DMF solutions, leading to a substantial improvement in overall conversion yields without interference from water or proton reduction.

Keywords: oxidative reduction, mediated oxalate oxidation, carbon dioxide radical anion, hydrodehalogenation, bulk electrolysis

TOC:

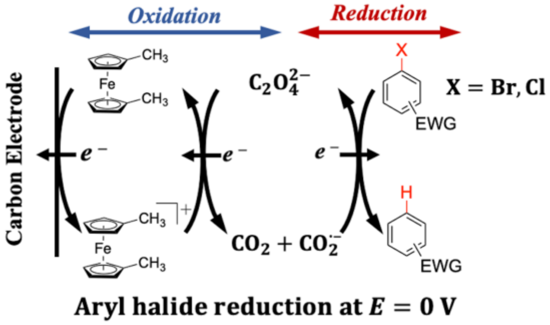

Introduction

Despite significant progress in the field of electrosynthesis, advances in anodic oxidations far outpace advances in cathodic reductions.[1-3] In part, this disparity can be attributed to the wide array of oxidizing redox mediators (i.e., cyclopropeniums,[4] N-oxyl radicals,[5] triarylamines,[6] halogenide salts,[7] and metal salts[8]) that are available compared to reducing redox mediators, which are generally limited to Ni-salen,[9] Co-salen,[10] fullerenes,[11] and aromatic hydrocarbons.[12] Anodic oxidations are also conveniently paired with the hydrogen evolution reaction (HER) as the supporting half reaction, while cathodic reductions typically make use of a sacrificial anode, a component that is susceptible to passivation or results in the introduction of unwanted chemical species.[3, 13, 14] In addition, cathodic reductions often require electrode potentials far beyond the formal potential for proton and water reduction, requiring dry organic solvents and maintaining a moisture-free environment.[3, 15] This report offers a simple electroorganic synthesis strategy to address all of these concerns.

In-situ generation of the carbon dioxide radical anion ($CO_2^{\bullet-}$) using mild reaction conditions is a general goal for the activation of organic molecules.[16] $CO_2^{\bullet-}$ can be accessed photochemically via hydrogen-atom abstraction from formate (HCO_2^-) or electrochemically by CO_2 reduction.[16] Once generated, $CO_2^{\bullet-}$ enables a variety of follow-up organic reactions, including hydrodehalogenation,[17-19] carboarylation,[20-22] oxyarylation,[23] radical deamination,[17, 18] aldehyde reduction,[17] Birch reduction,[24] sulfonamide cleavage,[17, 19] and the carboxylation (or decarboxylation) of a wide variety of unsaturated C–C bonds.[17, 25-31] In each of the aforementioned examples, $CO_2^{\bullet-}$ functions either as a single electron transfer (SET) reductant or as a nucleophile, depending on the formal reduction potential ($E^{0'}$) and the electrophilicity of the organic substrate. If $E^{0'}$ of the organic substrate is positive of $E^{0'}(CO_2/CO_2^{\bullet-}) = -2.68$ V vs $E^{0'}$ of Fc/Fc^+ in DMF,[32] then SET from $CO_2^{\bullet-}$ to the organic substrate is thermodynamically allowed. Alternatively, if $E^{0'}$ of the organic substrate is negative of $E^{0'}(CO_2/CO_2^{\bullet-})$, SET is thermodynamically prohibited. In the latter scenario, $CO_2^{\bullet-}$ may act as a nucleophile to a sufficiently electrophilic organic substrate, as is the case for unsaturated C–C bonds.

At least fifty reports of photochemically generated $CO_2^{\bullet-}$ applied to organic synthesis have appeared in the literature during the past seven years.[16] In the same time frame, however, less than a dozen reports of electrochemically generated $CO_2^{\bullet-}$ for organic synthesis are available.[33-40] Additionally, the electrochemical methods are all based on direct CO_2 reduction to form $CO_2^{\bullet-}$, necessitating cathode potentials in excess of –2.5 V vs Fc/Fc^+.

A concept for electrochemical $CO_2^{\bullet-}$ generation for small molecule activation at a low electrode potential is found in the literature describing co-reactant electrogenerated chemiluminescence (ECL). Briefly, a seminal work by Bard and co-workers utilized the oxidation of rubrene in the presence of $C_2O_4^{2-}$ (the co-reactant) to generate ECL.[41] The oxidation of rubrene to the rubrene radical cation at $E \approx 0.4$ V vs Fc/Fc^+ results in homogeneous oxidation of $C_2O_4^{2-}$ to $CO_2^{\bullet-}$, which is capable of reducing rubrene to the rubrene radical anion ($E \approx -1.7$ V vs Fc/Fc^+).[42-47] Electron-transfer between the radical cation and radical anion of rubrene yields excited state rubrene that emits a photon.

Herein, we describe the redox mediated *oxidation* of $C_2O_4^{2-}$ to generate $CO_2^{\bullet-}$ for the *reduction* of aryl halides, Ar–X (X = Br, Cl), eqs 1–4.

$$\text{Ar–X} + CO_2^{\bullet-} \rightarrow \text{Ar–X}^{\bullet-} + CO_2 \qquad (1)$$

$$\text{Ar–X}^{\bullet-} \rightarrow \text{Ar}^{\bullet} + \text{X}^{-} \qquad (2)$$

$$\text{Ar}^{\bullet} + CO_2^{\bullet-} \rightarrow \text{Ar}^{-} + CO_2 \qquad (3)$$

$Ar^{-} + H^{+} \rightarrow Ar{-}H$ (4)

Since the $CO_2^{\bullet-}$ in reaction 1 results from mediated $C_2O_4^{2-}$ oxidation at an anode, we refer to this method as "oxidative reduction" or, equivalently, "reduction by oxidation." Cyclic voltammetry is first employed to examine the feasibility of the oxidative reduction method. Then, we demonstrate that efficient conversion of Ar–X (X = Br, Cl) to Ar–H (i.e., reductive hydrodehalogenation) in controlled-potential electrolysis is achieved in < 4 h at very moderate potentials (~ 0 V vs Fc/Fc^{+}). This method, where a reduction is carried out in the anode compartment, uses HER as the counter-electrode reaction, eliminating the need for a sacrificial anode. Furthermore, additions of H_2O are used to optimize the conversion yield, demonstrating that rigorous drying of the solvent and supporting electrolyte is not required for hydrodehalogenation. Lastly, finite difference simulations are used to gain insight into the oxidative reduction mechanism.

Results and Discussion

Electrochemical oxidation of $C_2O_4^{2-}$ in DMF at glassy carbon (GC) electrodes yields 2 CO_2 molecules via an ECE mechanism, eqs 5–7.[47, 48]

$C_2O_4^{2-} \rightarrow C_2O_4^{\bullet-} + e^{-}$ $E^0 = -0.41$ V vs Fc/Fc^{+} (5)

$C_2O_4^{\bullet-} \rightarrow CO_2 + CO_2^{\bullet-}$ $k_f = 5.5 \times 10^5\ s^{-1}$ (6)

$CO_2^{\bullet-} \rightarrow CO_2 + e^{-}$ $E^0 = -2.68$ V vs Fc/Fc^{+} (7)

Upon formation of CO_2 by eqs 6 and 7, an electroactive adduct, $C_2O_4^{2-}{\bullet}CO_2$, is generated in dry DMF solutions, eq 8, which also undergoes 1e⁻ oxidation, eq 9, followed by dissociation, eq 10.[48, 49]

$$C_2O_4^{2-} + CO_2 \rightarrow C_2O_4^{2-}{\bullet}CO_2 \qquad (8)$$

$$C_2O_4^{2-}{\bullet}CO_2 \rightarrow C_2O_4^{\bullet-}{\bullet}CO_2 + e^- \qquad (9)$$

$$C_2O_4^{\bullet-}{\bullet}CO_2 \rightarrow C_2O_4^{\bullet-} + CO_2 \qquad (10)$$

As discussed in detail below, $C_2O_4^{2-}{\bullet}CO_2$ oxidation occurs at a potential ~ 0.5 V more positive than $C_2O_4^{2-}$ oxidation (i.e., $C_2O_4^{2-}{\bullet}CO_2$ is more stable than $C_2O_4^{2-}$ toward oxidation). Note that $C_2O_4^{\bullet-}{\bullet}CO_2$ has never been directly observed by means other than electrochemical measurements. However, coulometric analysis in our lab (*vide infra*) demonstrates that $C_2O_4^{2-}{\bullet}CO_2$ oxidation occurs by the overall transfer of $2e^-$. $C_2O_4^{2-}{\bullet}CO_2$ oxidation, eq 9, yields the oxidized adduct, $C_2O_4^{\bullet-}{\bullet}CO_2$, which rapidly decomposes to CO_2 and $C_2O_4^{\bullet-}$, eq 10. Then, $C_2O_4^{\bullet-}$ decomposes, eq 6, followed by oxidation of $CO_2^{\bullet-}$, eq 7. The overall $2e^-$ oxidation of $C_2O_4^{2-}{\bullet}CO_2$, obtained by summation of eqs 9, 10, 6, and 7 is given by eq 11.[49] In the present report, we demonstrate that the mediated $1e^-$ oxidations of $C_2O_4^{2-}$ and $C_2O_4^{2-}{\bullet}CO_2$ both generate $CO_2^{\bullet-}$ *in-situ*, which subsequently and efficiently reduces electron-deficient aryl halides according to eq 1.

$$C_2O_4^{2-}{\bullet}CO_2 \rightarrow 3CO_2 + 2e^- \qquad (11)$$

4-Bromobenzonitrile (4-BrBN) was selected as a model substrate for the oxidative reduction method as: (1) SET from $CO_2^{\bullet-}$ to 4-BrBN is thermodynamically allowed; (2) the reactions following 4-BrBN reduction occur rapidly to yield the product, benzonitrile (BN); and (3) BN is thermodynamically stable toward further reduction by $CO_2^{\bullet-}$.

A cyclic voltammogram (CV) for the direct reduction of 4-BrBN at a GC electrode in dry DMF is shown by the black trace in Figure 1A where the first reduction wave at ~ –2.4 V corresponds to the irreversible $2e^-$ reduction of 4-BrBN to generate BN. This irreversible reduction is followed by the reversible reduction of BN ($BN + e^- \rightleftarrows BN^{\bullet-}$, $E^{0'} = -2.74$ V). All CV studies used a three-electrode cell consisting of a GC working electrode, Pt wire counter electrode, and Ag/Ag_xO quasi-reference electrode (QRE) that was calibrated vs the Fc/Fc^+ redox couple.

Direct $C_2O_4^{2-}$ oxidation at a GC electrode (red curve in Figure 1A) first follows an ECE mechanism, eqs 5–7, corresponding to the first voltammetric wave beginning near $E = -0.50$ V. As CO_2 is generated from $C_2O_4^{2-}$ oxidation, $C_2O_4^{2-}{\bullet}CO_2$ forms in solution via eq 8, resulting in the appearance of a second oxidation wave near 0 V that is described by eqs 9 and 10 followed by eqs 6 and 7.

Theoretically, direct $C_2O_4^{2-}$ oxidation can generate $CO_2^{\bullet-}$ that is capable of reducing 4-BrBN; however, this method is highly inefficient, *vide infra*, due to rapid oxidation of $CO_2^{\bullet-}$ at the working electrode. Upon the transfer of a single electron from $C_2O_4^{2-}$ to the electrode, the resulting $C_2O_4^{\bullet-}$ decomposes to CO_2 and $CO_2^{\bullet-}$ within 1.2 μs, eq 6.[47] Using $\delta = (2Dt)^{1/2}$, where δ is the distance $C_2O_4^{\bullet-}$ diffuses from the electrode, D is the diffusion coefficient of $C_2O_4^{\bullet-}$ (5.0×10^{-6} cm^2/s) and t is the lifetime of $C_2O_4^{\bullet-}$ (1.2 μs), one can estimate that $CO_2^{\bullet-}$ is formed from $C_2O_4^{\bullet-}$ dissociation within $\sim 3\delta \sim 100$ nm of the electrode surface, where it is rapidly oxidized, eq 7.[50] Thus, the likelihood that $CO_2^{\bullet-}$ encounters and reduces 4-BrBN before being oxidized at the electrode is very low, a prediction supported by bulk electrolysis studies showing that less than 5% of 4-BrBN is converted to BN upon direct $C_2O_4^{2-}$ oxidation, *vide infra*.

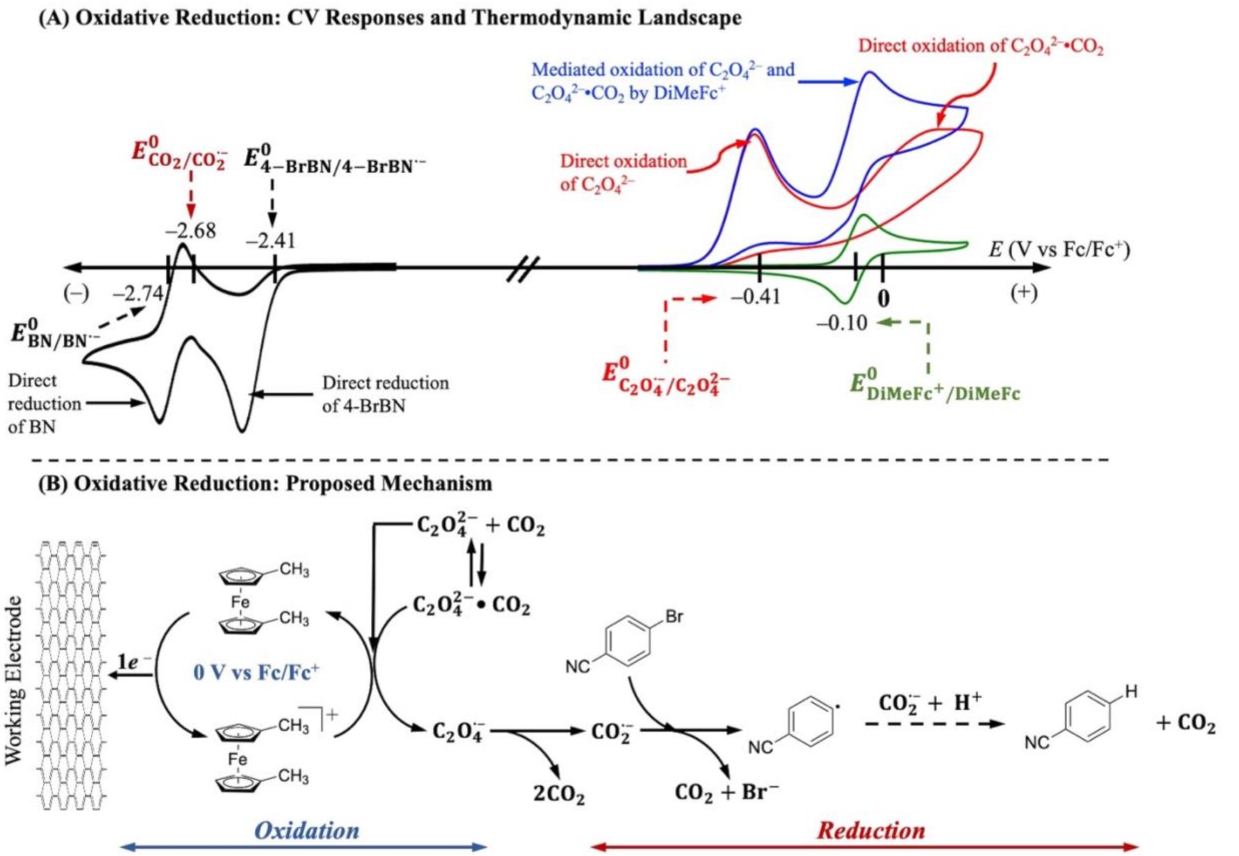

Figure 1. (A) Voltammetric responses and values of the standard redox potentials (E^0) for 4-BrBN reduction (black), $C_2O_4^{2-}$ and $C_2O_4^{2-}$•CO_2 oxidation (red), 1,1-dimethylferrocene (DiMeFc) oxidation (green), and $DiMeFc^+$-mediated $C_2O_4^{2-}$ oxidation (blue). (B) Proposed mechanism for the mediated oxidative reduction of 4-BrBN at potentials where $DiMeFc^+$ is capable of oxidizing $C_2O_4^{2-}$ and $C_2O_4^{2-}$•CO_2. All CVs were collected in an O_2-free DMF solution containing 0.1 M TBAP supporting electrolyte at ν = 100 mV/s.

The outer-sphere redox mediator, 1,1-dimethylferrocene (DiMeFc), was employed to mitigate direct heterogenous $CO_2^{\bullet-}$ oxidation at the electrode. DiMeFc undergoes a reversible one-electron oxidation at E^0 = –0.10 V vs Fc/Fc$^+$, eq 12 (Figure 1A, green trace).

$$\text{DiMeFc} \rightleftarrows \text{DiMeFc}^+ + e^- \qquad E^0 = -0.10 \text{ V vs Fc/Fc}^+ \qquad (12)$$

In the presence of $C_2O_4^{2-}$, a large increase in the anodic peak current (i_{pa}) associated with DiMeFc oxidation is observed, which is accompanied by disappearance of the $DiMeFc^+$ reduction peak. Both observations are indicative of $DiMeFc^+$-mediated $C_2O_4^{2-}$ oxidation, eq 13 (Figure 1A, blue trace).

$$DiMeFc^+ + C_2O_4^{2-} \rightleftarrows DiMeFc + C_2O_4^{\bullet-} \tag{13}$$

The mediation mechanism, however, is not immediately obvious as direct $C_2O_4^{2-}$ oxidation occurs at a potential that is ~0.4 V less positive than DiMeFc oxidation and is unaffected by the presence of DiMeFc. Mediated oxidation of $C_2O_4^{2-}$ occurs upon oxidation of DiMeFc, which also overlaps with the oxidation of $C_2O_4^{2-}{\bullet}CO_2$. Thermodynamically, both $C_2O_4^{2-}$ and $C_2O_4^{2-}{\bullet}CO_2$ can be oxidized by $DiMeFc^+$ via eqs 13 and 14, respectively. Note that eq 14 is equivalent to the sum of

$$DiMeFc^+ + C_2O_4^{2-}{\bullet}CO_2 \rightleftarrows DiMeFc + C_2O_4^{\bullet-}{\bullet}CO_2 \tag{14}$$

the reverse of eq 8, $C_2O_4^{2-}{\bullet}CO_2$ dissociation into $C_2O_4^{2-}$ and CO_2, and eq 13, the homogeneous oxidation of $C_2O_4^{2-}$ by $DiMeFc^+$ and the reverse of eq 10, association of $C_2O_4^{\bullet-}$ and CO_2 to form $C_2O_4^{\bullet-}{\bullet}CO_2$. In this scenario, eq 14 is not explicitly required to describe the overall mediation mechanism. However, CV studies and finite-difference simulations presented later support the occurrence of eq 14. Regardless of the mediation pathway, $C_2O_4^{\bullet-}$ forms and rapidly decomposes into CO_2 and $CO_2^{\bullet-}$, eq 6. $CO_2^{\bullet-}$ is then capable of reducing $DiMeFc^+$, eq 15.

$$DiMeFc^+ + CO_2^{\bullet-} \rightarrow DiMeFc + CO_2 \tag{15}$$

The net result is two parallel pathways by which mediated $C_2O_4^{2-}$ oxidation occurs: (1) eq 12 followed by eqs 13, 6, 15, and 12 and (2) eq 12 followed by eqs 14, 10, 6, 15, and 12. Pathway 1 represents a 5-step EC'CCE mechanism resulting in the $2e^-$ oxidation of $C_2O_4^{2-}$ to $2CO_2$. Pathway 2 follows a 6-step EC'CCCE mechanism that yields the $2e^-$ oxidation of $C_2O_4^{2-}{\bullet}CO_2$ to $3CO_2$. Note that addition of eq 8 to Pathway 2 yields the $2e^-$ oxidation of $C_2O_4^{2-}$ to $2CO_2$, demonstrating that both pathways are equivalent. Hereafter, for simplicity, we refer to the combination of both pathways as $DiMeFc^+$-mediated $C_2O_4^{2-}$ oxidation.

As shown in Figure 2, the anodic peak current (i_{pa}) associated with direct $C_2O_4^{2-}$ oxidation is unaffected by the presence of 4-BrBN, within the error of the measurement. However, the addition of 4-BrBN results in a substantial decrease in i_{pa} for $DiMeFc^+$-mediated $C_2O_4^{2-}$ oxidation. The finding that direct $C_2O_4^{2-}$ oxidation is unchanged upon introducing 4-BrBN to the solution supports the prediction that $CO_2^{\bullet-}$ generated from direct $C_2O_4^{2-}$ oxidation is immediately oxidized at the electrode, effectively preventing the reduction of 4-BrBN by $CO_2^{\bullet-}$. Conversely, the decrease in i_{pa} for $DiMeFc^+$-mediated $C_2O_4^{2-}$ oxidation can be attributed to the homogeneous reduction of 4-BrBN by $CO_2^{\bullet-}$, preventing both direct $CO_2^{\bullet-}$ oxidation (eq 7) as well as the regeneration and subsequent oxidation of DiMeFc (eq 15 followed by eq 12). CV studies presented in the Supporting Information rule out: (1) 4-BrBN adsorption (Figure S1); (2) reduction of 4-BrBN via $CO_2^{\bullet-}$ generated from direct $C_2O_4^{2-}{\bullet}CO_2$ oxidation (Figure S2); (3) a chemical reaction between DiMeFc and $C_2O_4^{2-}$ (Figure S3A); or (4) a chemical reaction between 4-BrBN and either DiMeFc or $C_2O_4^{2-}$ (Figure S3B) as the origin of the decrease in i_{pa}. An expanded data set corresponding to the CVs shown in Figure 2 is presented in Figure S4.

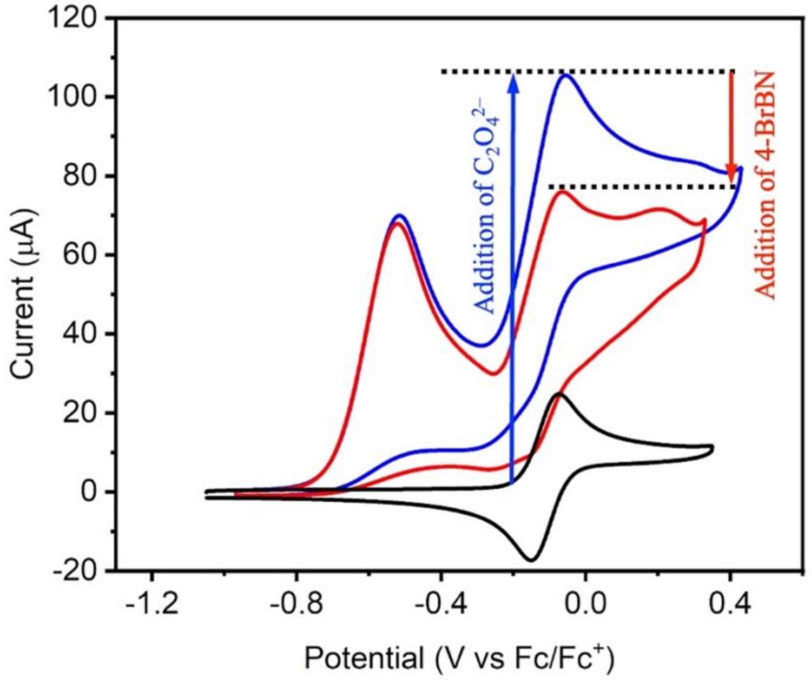

Figure 2. CV study of solutions containing 1.2 mM DiMeFc (black); 1.2 mM DiMeFc and 6.0 mM $C_2O_4^{2-}$ (blue); and 1.2 mM DiMeFc, 6.0 mM $C_2O_4^{2-}$, and 20 mM 4-BrBN (red). All CVs were carried out in an O_2-free DMF solution containing 0.1 M TBAP supporting electrolyte at υ = 100 mV/s.

The origin of the small voltammetric peak at ~0.2 V vs Fc/Fc$^+$ in the presence of 4-BrBN is either due to direct $C_2O_4^{2-}$•CO_2 oxidation (Figure S5) and/or Br^- oxidation (Figure S6), where Br^- is generated from 4-BrBN reduction, eqs 1 and 2. Specifically, in a DMF solution containing $C_2O_4^{2-}$, direct $C_2O_4^{2-}$•CO_2 oxidation occurs at ~0.2 V, while Br^- oxidation in a DMF solution containing only tetraethylammonium bromide also occurs at ~0.2 V. As such, the oxidation of both species may be responsible for the small voltammetric peak at ~0.2 V seen in the red trace in Figure 2. The products formed from Br^- oxidation, i.e., Br_2 and Br_3^-, are capable of oxidizing $C_2O_4^{2-}$ and DiMeFc and are susceptible to reduction by $CO_2^{\bullet-}$. However, Br_2 and Br_3^- are not generated until ~0.3 V positive of the anodic peak potential associated with DiMeFc$^+$-mediated $C_2O_4^{2-}$ oxidation. As such, these reactions do not impact the voltammetric responses associated with DiMeFc$^+$-mediated $C_2O_4^{2-}$ oxidation and the follow-up reduction of 4-BrBN by $CO_2^{\bullet-}$ and are therefore ignored in the mechanistic analysis presented later. In addition, the potential applied during bulk electrolysis is not sufficiently positive to oxidize Br^-.

Mediated Oxidative Reduction in a Saturated CO_2 Solution

By saturating a DMF solution with CO_2, $C_2O_4^{2-}$ is expected to exist almost exclusively as $C_2O_4^{2-}\bullet CO_2$, eq 8.[48, 49] In this way, the voltammetric behavior of $C_2O_4^{2-}\bullet CO_2$ can be examined independent of free $C_2O_4^{2-}$ in solution. Addition of DiMeFc to a CO_2-saturated solution containing $C_2O_4^{2-}$ can then be used to determine whether eq 14 occurs. Furthermore, successful oxidative reduction of 4-BrBN in a saturated CO_2 solution can provide evidence that $CO_2^{\bullet-}$ is generated through the course of $C_2O_4^{2-}\bullet CO_2$ oxidation.

Figure 3A shows CVs for the oxidation of 6.0 mM $C_2O_4^{2-}$ where CO_2 is initially absent (black) or initially present at its saturation concentration, 0.23 M at 1 atm in DMF (red).[51] Voltammograms identical to those shown in Figure 3A, first reported by Maran and co-workers, were used to establish $C_2O_4^{2-}\bullet CO_2$ oxidation as the origin of the CV wave observed near 0.15 V vs Fc/Fc$^+$.[48] Finite-difference simulations and *ab initio* molecular dynamics simulations from our lab demonstrate that, in the presence of 0.23 M CO_2, all $C_2O_4^{2-}$ (initially present at 6.0 mM) is bound to CO_2 to form the $C_2O_4^{2-}\bullet CO_2$ adduct.[49]

As such, CV experiments analogous to those presented in Figure 2 were repeated in CO_2-saturated DMF solutions, Figure 3B. The black curve in Figure 3B, corresponding to a CV of 1.2 mM DiMeFc in the presence of 0.23 M CO_2, is unchanged with respect to the CV of DiMeFc in the absence of CO_2 (Figure 2), demonstrating, as expected, that CO_2 does not chemically interact with DiMeFc or DiMeFc$^+$. Addition of 6.0 mM $C_2O_4^{2-}$ (Figure 3B, blue) results in an increase in

i_{pa} for DiMeFc oxidation and the absence of a cathodic wave for $DiMeFc^+$ reduction. Because $C_2O_4^{2-}{\bullet}CO_2$, and not $C_2O_4^{2-}$, exists in the CO_2-saturated solution, the results shown in Figure 3B indicate that $DiMeFc^+$ mediates the oxidation of $C_2O_4^{2-}{\bullet}CO_2$, eq 14. Simulations presented in the Mechanistic Analysis Section demonstrate that eq 14 is explicitly required to successfully model experimental CV responses.

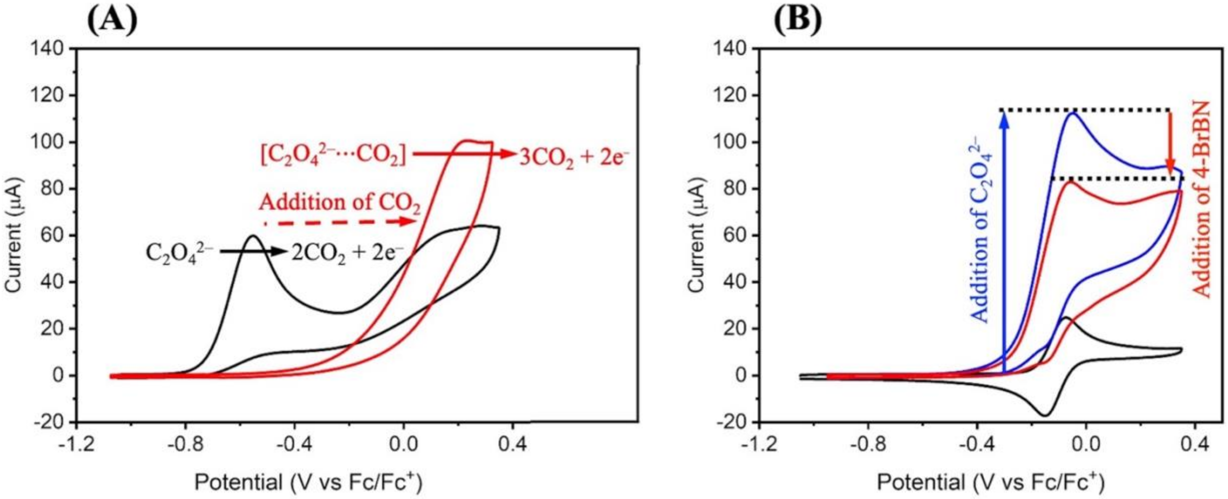

Figure 3. (A) CV study of a DMF solution containing 6.0 mM $C_2O_4^{2-}$ in the absence (black trace) and presence (red trace) of CO_2, where CO_2 (1 atm) was bubbled into the solution for 15 min between scans. (B) CV study of a CO_2-saturated DMF solution containing 1.2 mM DiMeFc (black trace);1.2 mM DiMeFc and 6.0 mM $C_2O_4^{2-}$ (blue trace); and 1.2 mM DiMeFc, 6.0 mM $C_2O_4^{2-}$, and 20 mM 4-BrBN (red trace). All CVs were collected in an O_2-free DMF solution containing 0.1 M TBAP supporting electrolyte at $\nu = 100$ mV/s.

A decrease in i_{pa} is observed in the presence of 4-BrBN (Figure 3B, red), indicating the reduction of 4-BrBN by $CO_2^{\bullet-}$ produced by the mediated oxidation of $C_2O_4^{2-}{\bullet}CO_2$, analogous to the red curve in Figure 2. An expanded data set for Figure 3B is presented in Figure S7. Furthermore, bulk electrolysis using the mediated oxidative reduction method in a CO_2-saturated DMF solution results in the quantitative reduction of 4-BrBN to BN, *vide infra* and Figure S18.

DiMeFc$^+$-mediated $C_2O_4^{2-}$•CO_2 oxidation therefore generates $CO_2^{\bullet-}$ in solution (eq 14 followed by eqs 6 and 10), which enables the rapid and irreversible reduction of 4-BrBN.

Oxidative Reduction in the Presence of H_2O

In aprotic solvents such as acetonitrile and DMF, addition of a weakly acidic hydrogen-bond donor such as H_2O is known to result in a positive shift in the anodic peak potential (E_{pa}) for $C_2O_4^{2-}$ oxidation, a consequence of the stabilization of $C_2O_4^{2-}$ (a hydrogen-bond acceptor) by H_2O (a hydrogen-bond donor).[48] The top panel in Figure 4A demonstrates that sequential additions of H_2O to a DMF solution containing $C_2O_4^{2-}$ enables fine-tuning of E_{pa} for $C_2O_4^{2-}$ oxidation over a 700 mV range. As E^0(DiMeFc$^+$/DiMeFc) lies between the lower- and upper-limits of this range (Figure 4A, bottom panel, black), we hypothesized that DiMeFc$^+$-mediated $C_2O_4^{2-}$ oxidation can be optimized by additions of H_2O to the solution, where the driving force for DiMeFc$^+$-mediated $C_2O_4^{2-}$ oxidation approximately depends on E_{pa} for $C_2O_4^{2-}$ oxidation relative to E^0(DiMeFc$^+$/DiMeFc). Note that, in the presence of 8 M H_2O, E^0(DiMeFc$^+$/DiMeFc) shifts only –70 mV (see bottom panel of Figure 4A), and the current for the reversible 1e$^-$ oxidation of DiMeFc decreases due to an increase in solution viscosity (see Figure S8 and the accompanying text).

To test this hypothesis, CVs of 0.9 mM DiMeFc and 5.0 mM $C_2O_4^{2-}$ were recorded as a function of the concentration of H_2O added to the solution, Figure 4B. In the absence of H_2O (black), a CV identical in shape to the one shown in blue in Figure 2 is obtained. In the presence of 1 M water (red), the expected shift in E_{pa} for direct $C_2O_4^{2-}$ oxidation is observed, while i_{pa} for both direct and DiMeFc$^+$-mediated $C_2O_4^{2-}$ oxidation increases in magnitude, suggesting an enhancement in mediated $C_2O_4^{2-}$ oxidation. A single oxidation peak with nearly identical values of i_{pa} is observed in the presence of 2 (blue) and 4 M (orange) H_2O. When 8 M H_2O is present in the solution (green), i_{pa} decreases, the cathodic peak associated with DiMeFc$^+$ reduction reappears, and direct $C_2O_4^{2-}$ oxidation is observed ~0.2 V positive of DiMeFc oxidation. Figure S9 provides a comparison between direct and mediated $C_2O_4^{2-}$ oxidation at eight H_2O concentrations between 0 and 8 M.

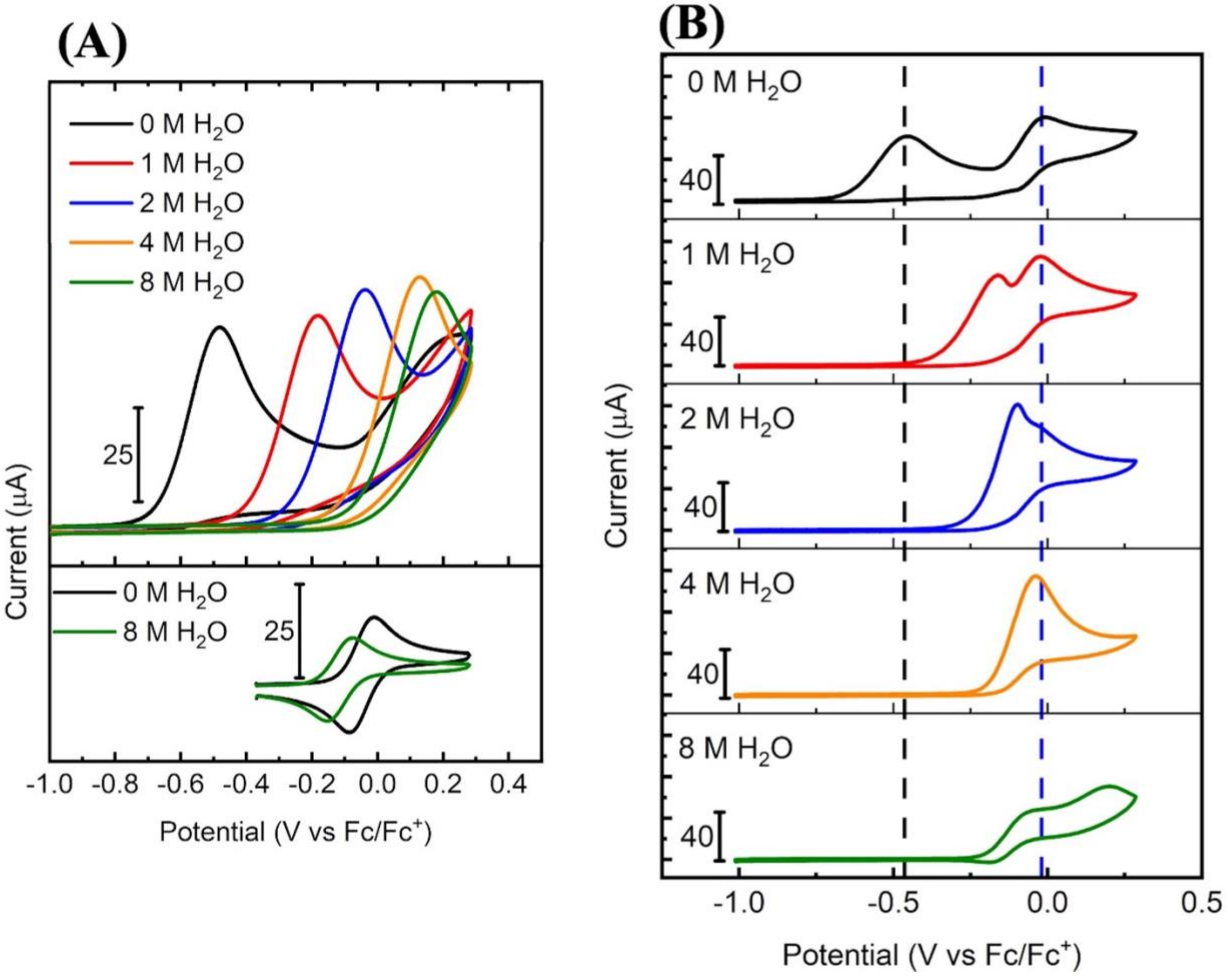

Figure 4. (A) Top panel: CV study of a DMF solution containing 5.0 mM $C_2O_4^{2-}$ in the presence of 0 (black), 1 (red), 2 (blue), 4 (orange), and 8 (green) M H_2O. Bottom inset: CVs of 0.9 mM DiMeFc in the presence of 0 (black) and 8 (green) M H_2O. (B) CVs of a DMF solution containing 0.9 mM DiMeFc **and** 5.0 mM $C_2O_4^{2-}$ in the presence of 0 (black), 1 (red), 2 (blue), 4 (orange), and 8 (green) M H_2O. The black dashed line represents E_{pa} for direct $C_2O_4^{2-}$ oxidation in the absence of H_2O, while the blue dashed line corresponds to E_{pa} for DiMeFc$^+$-mediated $C_2O_4^{2-}$ oxidation in the absence of H_2O. All CVs were collected in an O_2-free DMF solution containing 0.1 M TBAP supporting electrolyte at ν = 100 mV/s.

Figure 4B shows that the rate of DiMeFc$^+$-mediated $C_2O_4^{2-}$ oxidation depends strongly on the concentration of H_2O present in solution. Typically, mediators with different E^0 values are screened to tune the rate of homogeneous redox mediation toward a single substrate. Alternatively, the results in Figure 4B show that, using a single mediator, the rate of homogeneous redox mediation is altered by altering the redox potential of the substrate via the introduction of an additive (H_2O). It is straightforward to hypothesize that the efficiency of $CO_2^{\bullet-}$ generation, and, by extension, the follow-up reduction of 4-BrBN, can be tuned by controlling the H_2O content of the system, an idea explored in the following section.

Preparative-Scale Hydrodehalogenation of Electron-Deficient Aryl Bromides and Aryl Chlorides in Mixed DMF-H_2O Electrolytes

CVs presented in Figures 2 and 3B suggest that $CO_2^{\bullet-}$ generated by DiMeFc$^+$-mediated $C_2O_4^{2-}$ oxidation undergoes a homogeneous chemical reaction with 4-BrBN. Furthermore, Figures 4B and S10–S13 suggest that the efficiency of the mediated oxidative reduction of 4-BrBN depends on the concentration of H_2O present in the solution. As cyclic voltammetry provides little information regarding the reaction outcome, controlled-potential electrolysis (CPE) experiments were carried out to determine the final products. Details of the electrolysis cell, procedure, product isolation, and product characterization can be found in the Supporting Information. A brief summary of the CPE methodology is presented here.

All CPE experiments were performed in a divided cell where an ion permeable glass frit and methyl cellulose ion exchange membrane were used to separate the anolyte and catholyte, as described elsewhere.[52] A reticulated vitreous carbon (RVC) electrode and Ag/Ag$_x$O QRE were placed in the anolyte compartment, while a graphite rod electrode was placed in the catholyte compartment. The Ag/Ag$_x$O QRE was placed in a glass capillary filled with DMF/0.1 M TBAP and was separated from the anolyte solution by a glass frit. Glacial acetic acid (0.5 mL of 17 M to give 0.4 M acetic acid in DMF/0.1 M TBAP) was added to the catholyte compartment, enabling the hydrogen evolution reaction to serve as the cathode half-reaction.

Figure 5 shows a typical current–time (*i*–*t*) trace for the mediated oxidative reduction of 4-BrBN. Prior to the beginning of bulk electrolysis, 20 mL of a DMF solution containing 0.1 M TBAP and 1.0 M H_2O (i.e., the solvent composition is 19.64 mL DMF and 0.36 mL H_2O) was deaerated with Ar gas for 30 min to remove any dissolved O_2. Throughout the entirety of all CPE experiments, an Ar atmosphere was maintained over the solution headspace (Note: this CPE is air sensitive as $CO_2^{\bullet-}$ can reduce O_2 to $O_2^{\bullet-}$). Following the removal of O_2, a potential of 0.0 V vs Fc/Fc$^+$ was applied to the RVC anode, at which point a small charging current is observed, denoted by point (A) in Figure 5. Upon stabilization of the current to a steady baseline, 1 mL of deaerated solvent was removed from the anode compartment and was used to dissolve 4-BrBN (4 mg, 0.02 mmol). The concentrated 4-BrBN solution was then injected into the anode compartment, point (B) in Figure 5. As expected, no change in current is observed, demonstrating that 4-BrBN is not electroactive at 0.0 V. After 45 min, 2 mL of deaerated anolyte was removed from the cell, into which to DiMeFc (4 mg, 0.02 mmol) and $(TEA)_2C_2O_4$ (52 mg, 0.15 mmol) were dissolved. This concentrated solution was injected back into the anode compartment at point (C) in Figure 5, resulting in a large anodic current spike. After approximately 2 h, the current returned to its original baseline value, point (D), indicating conclusion of the electrolysis. Liquid-liquid extraction was used to isolate the resulting reaction products, which were analyzed by ultra-high-performance liquid chromatography/mass spectrometry (UHPLC/MS) and gas-chromatography/mass spectrometry (GC/MS) (see Supporting Information for additional details).

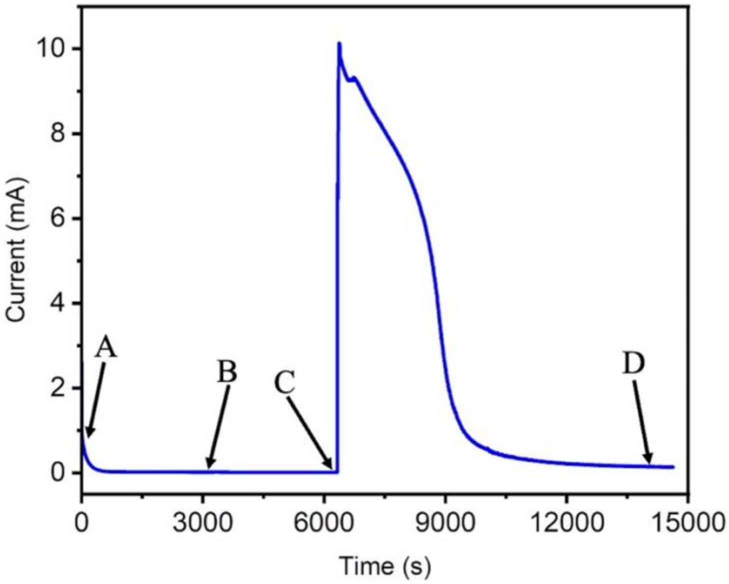

Figure 5. An example *i*-t trace of an electrolysis obtained in an O_2-free DMF solution containing 0.1 M TBAP supporting electrolyte, 1.0 M H_2O, 1.0 mM DiMeFc, 7.5 mM $C_2O_4^{2-}$, and 1.0 mM 4-BBN. (A) Application of E = 0.0 V vs Fc/Fc$^+$ to the working electrode; (B) addition of 4-BrBN; (C) addition of DiMeFc and $C_2O_4^{2-}$; (D) completion of the electrolysis.

Results for the oxidative reduction of 4-BrBN with five different DMF/H_2O solvent compositions are shown in Table 1. High conversion yields are achieved in the presence of 0, 1, and 2 M of H_2O (entries 1–3), while poor conversion yields are obtained in the presence of 4 and 8 M H_2O (entries 4 and 5). When 1 M H_2O is present in the solution, a 95% conversion yield is obtained, representing the approximate optimal solution condition for the oxidative reduction of 4-BrBN.

Table 1. Product distribution (mol %) for controlled-potential electrolysis of 1.0 mM 4-bromobenzonitrile in a DMF solution containing **1.0 mM DiMeFc, 7.5 mM $(TEA)_2C_2O_4$**, and 0.1 M TBAP at 0.0 V vs Fc/Fc^+.

No.	H_2O Concentration (M)	4-bromobenzonitrile	Benzonitrile
1	0	32	68
2	1	5	95
3	2	30	70
4	4	87	13
5	8	>95	<5

The results in Table 1 qualitatively agree with the hypothesis put forth from CV studies that the efficiency of the oxidative reduction of 4-BrBN is predictably tuned by additions of H_2O. Entries 1–3 in Table 1, corresponding to H_2O concentrations of 0, 1, and 2 M, are in good agreement with the CV data presented in Figures 2, S4, S10, and S11, where high conversion yields (CPE) are predicted by a significant decrease in the voltammetric i_{pa} in the presence of 4-BrBN (CV). Then, entry 5 in Table 1 agrees with the CV study shown in Figure S13, where the low conversion yield in the presence of 8 M H_2O, 5%, correlates to i_{pa} being unchanged upon addition of 4-BrBN, Figures 4B and S13.

Entry 4 in Table 1 gives an unexpected result when compared to the CV studies shown in Figures 4B and S12. A low (13%) conversion yield is obtained from CPE despite a decrease in i_{pa} that is comparable to solutions containing 0, 1 and 2 M H_2O where conversion yields are > 67%. As discussed above, H_2O can form intermolecular hydrogen-bonds with $C_2O_4^{2-}$ to form an $C_2O_4^{2-}$ •H_2O adduct, which likely inhibits the formation of $C_2O_4^{2-}$•CO_2.[48] The extent to which $C_2O_4^{2-}$ •CO_2 can form is therefore expected to be a strong function of the concentration of H_2O present in solution. We speculate that, if a sufficiently high quantity of H_2O is added to the solution, the formation of $C_2O_4^{2-}$•CO_2, eq 8, and, by extension, its homogeneous oxidation by DiMeFc$^+$, eq 14, will not occur with the net result being a decrease in $CO_2^{\bullet-}$ generation.

To examine the effect of H_2O on the stability of $C_2O_4^{2-}$•CO_2 and its follow-up oxidation by DiMeFc$^+$, CVs were recorded in CO_2-saturated DMF solutions containing DiMeFc, $C_2O_4^{2-}$, and increasing quantities of H_2O (Figure S14, black traces). Both reactions (eqs 8 and 14) are not perturbed when the concentration of $H_2O < 2$ M as nearly constant values of i_{pa} for the mediated oxidation of $C_2O_4^{2-}$•CO_2 are obtained in solutions containing 0, 1, and 2 M H_2O. Further additions of H_2O (Figure S14 D–H, black traces) result in a rapid decrease in i_{pa}, implying that the formation of $C_2O_4^{2-}$•H_2O inhibits $C_2O_4^{2-}$•CO_2 generation, eq 8, and thus the subsequent oxidation of $C_2O_4^{2-}$•CO_2 by DiMeFc$^+$, eq 14. To gain insight into how H_2O impacts the reduction of 4-BrBN by $CO_2^{\bullet-}$, the same experiment was repeated in the presence of 20 mM 4-BrBN (Figure S14, red traces). For solutions containing 0, 1, and 2 M H_2O, i_{pa} decreases by ~ 30% upon addition of 20 mM 4-BrBN, indicative of 4-BrBN reduction by $CO_2^{\bullet-}$. Conversely, i_{pa} is unaffected by the presence of 4-BrBN when the solution contains 4 M H_2O, suggesting that $CO_2^{\bullet-}$ formation is greatly inhibited. In summary, when the concentration of H_2O exceeds 2 M, $C_2O_4^{2-}$•H_2O formation prevents $C_2O_4^{2-}$•CO_2 from forming. As a result, three downstream reactions are inhibited: (1) homogeneous oxidation of $C_2O_4^{2-}$•CO_2 by DiMeFc$^+$ (eq 14); (2) the generation of $CO_2^{\bullet-}$ in solution (eq 10 followed by eq 6); (3) 4-BrBN reduction by $CO_2^{\bullet-}$ (eq 1). Entry 4 in Table 1, in combination with Figures S14 and S15, point to eqs 8 and 14 as essential elementary reactions in the oxidative reduction of 4-BrBN.

Under optimized conditions, the oxidation of 2.0 x 10^{-2} mmol DiMeFc and 1.5 x 10^{-2} mmol $(TEA)_2C_2O_4$ in the presence of 2.0 x 10^{-2} mmol 4-BrBN yields 1.1 x 10^{-2} mmol benzonitrile (BN) (the reduced product) and 6 x 10^{-4} mmol 4-BrBN (starting material), corresponding to a 95% conversion yield. Figure 6A provides a summary of the optimized reaction conditions, while Figures 6B and C present examples of electron deficient aryl bromides and chlorides, respectively, that underwent hydrodehalogenation using the oxidative reduction method. Each substrate shown in Figure 6 was selected based on E^0 of the substrate and its product relative to that of $CO_2^{\bullet-}$. Specifically, $E^0_{\text{substrate}} > E^0_{CO_2/CO_2^{\bullet-}}$ ensures that SET from $CO_2^{\bullet-}$ to the aryl halide substrate is thermodynamically allowed, while $E^0_{\text{product}} < E^0_{CO_2/CO_2^{\bullet-}}$ dictates that the product is stable towards further SET in the presence of $CO_2^{\bullet-}$. For example, the mediated oxidative reduction of bromobenzene in CPE does not occur as E^0 for this substrate is negative of $E^0(CO_2^{\bullet-}/CO_2)$, Figure S19. This result is consistent with the formation of bromobenzene upon mediated oxidative reduction of each of the three di-bromobenzene derivatives, Figure 6B.

Based on the products obtained in Figure 6, the overall redox reaction for the oxidative reduction of an aryl halide is described by eq 16.

$$\text{Ar–X} + 2C_2O_4^{2-} + H^+ \rightleftarrows \text{Ar–H} + X^- + 4CO_2 + 2e^- \qquad (16)$$

Our results suggest that the mechanism of hydrodehalogenation via oxidative reduction is consistent with the well-established mechanism for heterogeneous reductive hydrodehalogenation with $CO_2^{\bullet-}$ as the electron source, eqs 1–4.[53]

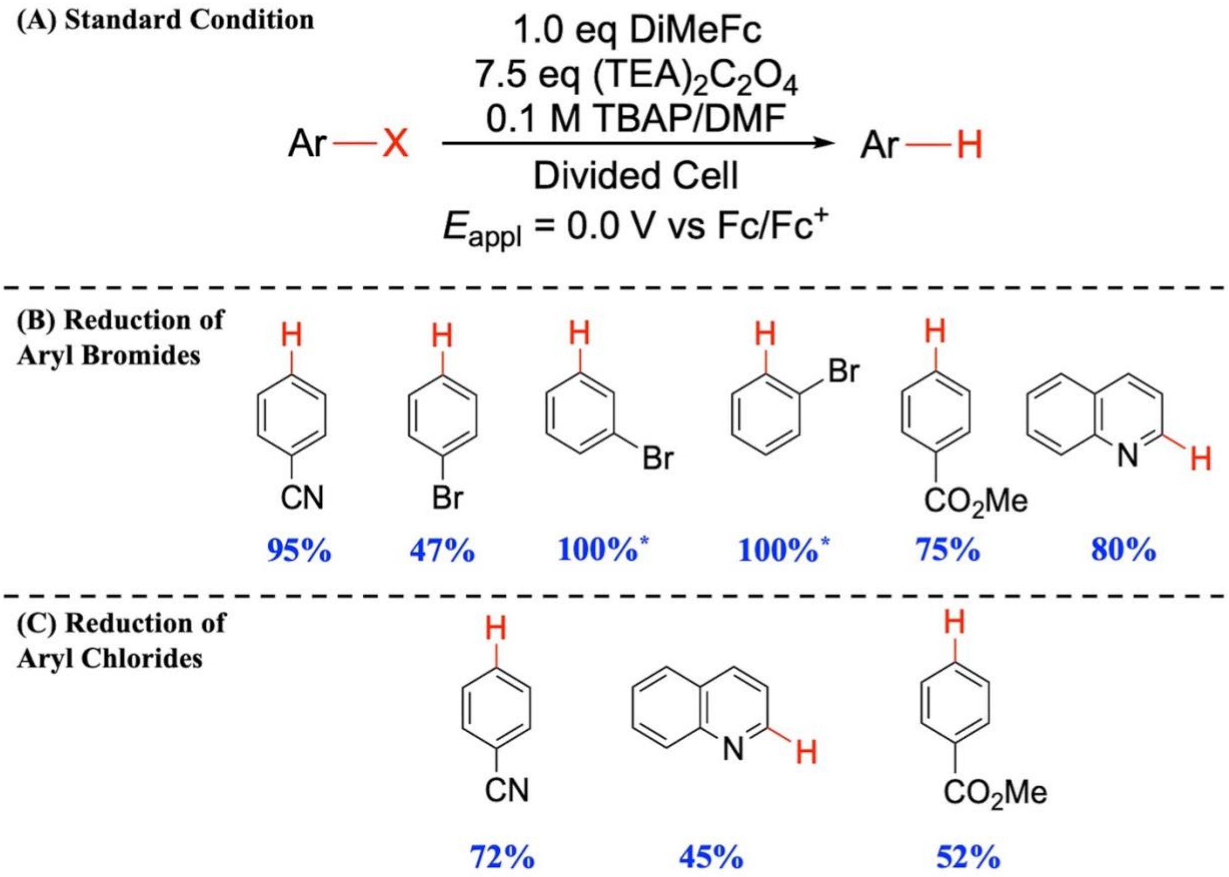

Figure 6. (A) Standard electrolysis conditions for the oxidative reduction of electron-deficient aryl bromides and aryl chlorides. (B) Examples of the hydrodehalogenation of electron-deficient aryl bromides. (C) Examples of the hydrodehalogenation of electron-deficient aryl chlorides. Values shown in blue refer to conversion yields that were computed as the ratio of product to starting material. See Supporting Information for a sample calculation of conversion yield. *Denotes that no starting material was detected.

Mechanistic Analysis

This section provides a more quantitative mechanistic analysis of DiMeFc$^+$-mediated $C_2O_4^{2-}$ oxidation and the follow-up reduction of 4-BrBN by $CO_2^{\bullet-}$. Finite-difference (FD) simulations (DigiSim®) were used to calculate CV responses based on kinetic, thermodynamic, and transport parameters for electrochemical and homogeneous chemical reactions under diffusive mass transport. Settings used for all simulations are described in the Supporting Information. For the sake of brevity, the following discussion is limited to the situation where external CO_2 and H_2O are not added to the solution.

Simulations for the mediated oxidative reduction of 4-BrBN (i.e., for a solution containing DiMeFc, $C_2O_4^{2-}$, and 4-BrBN) require a total of 44 parameters (i.e., diffusion coefficients, thermodynamic and rate parameters for heterogeneous and homogenous reactions). In general, fitting simulated voltammetric responses to experimental data using more than 3 or 4 adjustable parameters is an unreasonable task that often leads to non-unique values of the fitting parameters. As shown below, our simulation is greatly simplified by using 40 non-adjustable input parameters obtained either from the literature, from rigorous thermodynamic (Hess) calculations, or by reasonable assumptions, reducing the set of adjustable parameters to a reasonable number (four kinetic rate constants). The simplification of the simulations is discussed in more detail in the Supporting Information.

Simulations of mediated $C_2O_4^{2-}$ oxidation using DiMeFc/DiMeFc$^+$ in the absence of 4-BrBN were first considered. Figure 7 shows a comparison of experimental (solid lines) and simulated (dashed lines) voltammetric responses for solutions containing 0.9 mM DiMeFc and 0.0 (black), 2.2 (red), 5.5 (blue), and 7.5 (green) mM $C_2O_4^{2-}$. All thermodynamic, kinetic, and transport parameters used in these initial simulations are presented in Table S4. Table 2 shows rate constants for eqs 13–15 obtained in this work by fitting the simulations to experimental CVs. All CVs in Figure 7 correspond to a scan rate (υ) = 100 mV/s. Analogous results obtained at 50 and 250 mV/s are shown in Figures S23 and S25.

In the absence of $C_2O_4^{2-}$, a simple, reversible 1e$^-$ response associated with the DiMeFc$^{0/+}$ redox couple, eq 12, is obtained. The standard redox potential of DiMeFc$^{0/+}$ was measured as –0.10 V vs Fc/Fc$^+$, Figure S20. Values of the transfer coefficient (α) and heterogeneous rate constant

(k^0) of 0.5 and 0.97 ± 0.08 cm/s, respectively, have been reported in acetonitrile and were used without modification in the simulations, assuming a Butler-Volmer kinetic model.[54] A diffusivity (D) of 9.2×10^{-6} cm^2/s was used for both DiMeFc and DiMeFc$^+$ and is based on the reported value in acetonitrile of 1.94 (± 0.04) x 10^{-5} cm^2/s.[54] Details for adjusting D in acetonitrile to D in DMF based on solution viscosity are presented in the Supporting Information. For the moderate scan rates employed in this study, υ = 50 to 250 mV/s, a reversible CV typical of a diffusion-limited process is always obtained for a solution containing 0.9 mM DiMeFc, see Figure S21.

FD simulations of the voltammetric response for direct $C_2O_4^{2-}$ oxidation (eqs 5–10) are described elsewhere, with parameters obtained from that study shown in Table S4.[49] Upon addition of $C_2O_4^{2-}$ to the solution containing 0.9 mM DiMeFc, direct $C_2O_4^{2-}$ oxidation is observed in the simulations at ~ –0.5 V vs Fc/Fc$^+$, consistent with the experimental results shown in Figures 1A and 2.

Table 2. Simulation Parameters for the DiMeFc$^+$-mediated $C_2O_4^{2-}$ oxidation[a]

Eq No.	Reaction	K_{eq}	k_f
13	$DiMeFc^+ + C_2O_4^{2-} \rightleftarrows DiMeFc + C_2O_4^{\bullet-}$	1.7×10^5	$\leq 2 \times 10^6\ M^{-1}s^{-1}$
14	$DiMeFc^+ + C_2O_4^{2-}{\bullet}CO_2 \rightleftarrows DiMeFc + C_2O_4^{\bullet-}{\bullet}CO_2$	3.0×10^{-2}	$2.8 \times 10^3\ M^{-1}s^{-1}$
15	$DiMeFc^+ + CO_2^{\bullet-} \rightarrow DiMeFc + CO_2$	4.0×10^{43}	$10^6 – 10^{10}\ M^{-1}s^{-1}$

[a]Black: calculated from available thermodynamic data; green: determined from best fit of digital simulations to experimental CVs

Additions of $C_2O_4^{2-}$ result in an increase in the simulated i_{pa} associated with DiMeFc oxidation and the disappearance of the DiMeFc$^+$ reduction wave, consistent with electrogenerated DiMeFc$^+$ acting as a homogeneous redox mediator for $C_2O_4^{2-}$ and $C_2O_4^{2-}{\bullet}CO_2$ oxidation. A detailed mechanistic analysis and parameter optimization is presented in the Supporting

Information (Figures S26–S29). Comparison of simulated CVs to experiments yields the following key results: (1) mediated $C_2O_4^{2-}$•CO_2, eq 14, is required to obtain satisfactory agreement of simulated CVs with experimental data (Figure S26); (2) k_f^{14}, the rate constant for homogeneous $C_2O_4^{2-}$•CO_2 oxidation by $DiMeFc^+$ is equal to ~ 2.8 x 10^3 $M^{-1}s^{-1}$ (Figure S27); and (3) k_f^{13}, the rate constant for $DiMeFc^+$ oxidizing $C_2O_4^{2-}$, is ≤ 2 x 10^6 $M^{-1}s^{-1}$ (Figure S29). Optimized kinetic and thermodynamic parameters for the simulations shown in Figure 7 are given in Tables 2 and S4. Overall, these simulations are consistent with the mediation mechanism proposed following Figure 1 wherein $DiMeFc^+$ homogeneously oxidizes $C_2O_4^{2-}$ (eq 13) and $C_2O_4^{2-}$•CO_2 (eq 14) to regenerate DiMeFc and form $C_2O_4^{\bullet-}$, which produces $CO_2^{\bullet-}$ via eq 6. Once formed in solution, $CO_2^{\bullet-}$ can either undergo direct oxidation (eq 7) or reduce $DiMeFc^+$ (eq 15) to a second equivalent of DiMeFc that is then oxidized (eq 12).

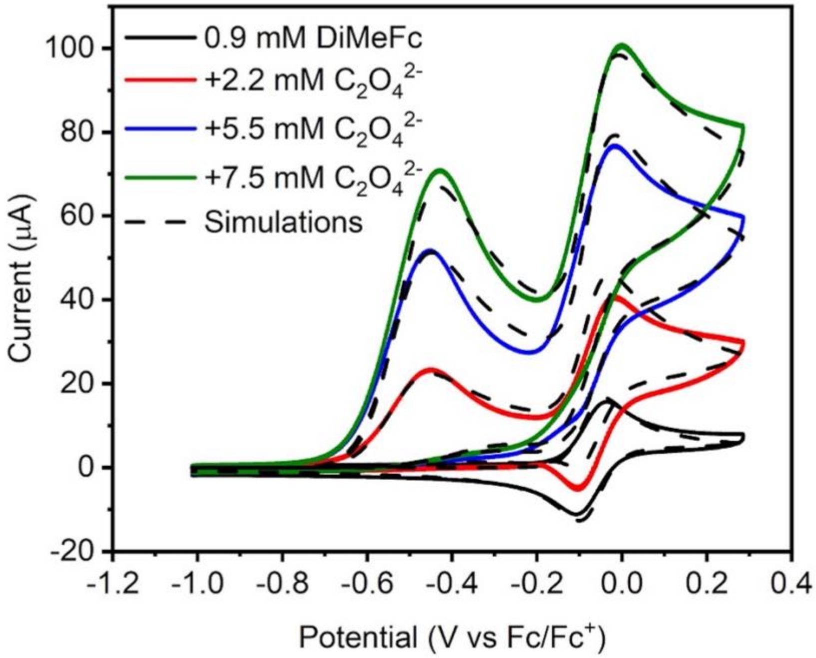

Figure 7. Experimental (solid lines) and simulated (dashed lines) CVs for solutions containing 0.9 mM DiMeFc (black), 0.9 mM DiMeFc and 2.2 (red), 5.5 (blue), or 7.5 (green) mM $C_2O_4^{2-}$. All voltammograms were collected in an O_2-free DMF solution containing 0.1 M TBAP supporting electrolyte at ν = 100 mV/s.

Details for the mechanism and parameters used for CV simulations can be found in the accompanying text as well as in Tables 2 and S4.

Simulated concentration distributions of $CO_2^{\bullet -}$ for direct $C_2O_4^{2-}$ oxidation and DiMeFc$^+$-mediated $C_2O_4^{2-}$ oxidation are compared in Figure 8 using simulation parameters optimized for CV responses, e.g., Figure 7. The curves shown in Figure 8 were extracted from a CV simulation at υ = 100 mV/s for a solution containing 0.9 mM DiMeFc and 5.5 mM $C_2O_4^{2-}$. The solid line corresponds to $E = -0.32$ V vs Fc/Fc$^+$, a potential where only direct $C_2O_4^{2-}$ oxidation occurs. The dashed line corresponds to $E = 0.03$ V vs Fc/Fc$^+$, a potential just past E_{pa} for DiMeFc$^+$-mediated $C_2O_4^{2-}$ oxidation. The corresponding concentration profiles for all other species included in the simulations (DiMeFc, DiMeFc$^+$, $C_2O_4^{2-}$, $C_2O_4^{2-}$•CO_2, CO_2, $C_2O_4^{\bullet -}$, $CO_2^{\bullet -}$, and $C_2O_4^{\bullet -}$•CO_2) at both potentials are shown in Figures S30 and S31.

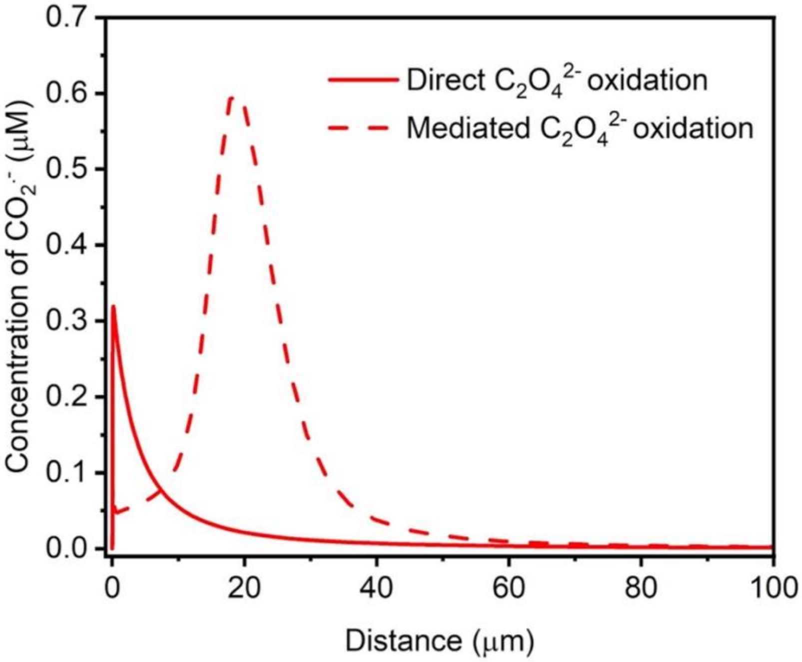

Figure 8. Simulated concentration profiles of $CO_2^{\bullet-}$ at $E = -0.32$ V vs Fc/Fc$^+$ (solid) and $E = 0.03$ V vs Fc/Fc$^+$ (dashed line). Both concentration profiles were collected from simulation of a solution containing 0.9 mM DiMeFc and 5.5 mM $C_2O_4^{2-}$ at $\upsilon = 100$ mV/s.

Figure 8 shows that when $C_2O_4^{2-}$ is directly oxidized, a maximum $CO_2^{\bullet-}$ concentration of 0.32 μM is obtained ~ 150 nm from the electrode surface. In contrast, DiMeFc$^+$-mediated $C_2O_4^{2-}$ oxidation results in a maximum $CO_2^{\bullet-}$ concentration of 0.60 μM at a distance of 20 μm from the electrode surface (Figure 8, dashed line), over two orders of magnitude further from the electrode surface compared to direct $C_2O_4^{2-}$ oxidation. These simulations are consistent with the use of a mediator to form $CO_2^{\bullet-}$ away from the electrode surface such that it can be used as a single electron reductant for homogeneous reductions in solution.

Experimental results presented in Figures 2 and S4 for the oxidation of $C_2O_4^{2-}$ and DiMeFc showed that the presence of 4-BrBN does not impact i_{pa} for direct $C_2O_4^{2-}$ oxidation but results in a substantial decrease in i_{pa} for DiMeFc$^+$-mediated $C_2O_4^{2-}$ oxidation. We ascribed this behavior to: (1) heterogeneous oxidation of $CO_2^{\bullet-}$ formed from direct $C_2O_4^{2-}$ oxidation, and (2) efficient homogeneous reduction of 4-BrBN by $CO_2^{\bullet-}$ generated from DiMeFc$^+$-mediated $C_2O_4^{2-}$ oxidation. As benzonitrile (BN) is the product detected following bulk electrolysis, eqs 17–20 are used to simulate the oxidative reduction of 4-BrBN. This 4-step mechanism follows the well-established ECEC mechanism for the electrochemical hydrodehalogenation of 4-BrBN, where the reductant, rather than being an electron from the cathode surface, is $CO_2^{\bullet-}$ generated at the anode by a mediation reaction.[55]

$$\text{4-BrBN} + CO_2^{\bullet-} \rightarrow \text{4-BrBN}^{\bullet-} + CO_2 \qquad (17)$$

$$\text{4-BrBN}^{\bullet-} \rightarrow \text{BN}^{\bullet} + \text{Br}^- \qquad (18)$$

$BN^{\bullet} + CO_2^{\bullet-} \rightarrow BN^{-} + CO_2$ (19)

$BN^{-} + H^{+} \rightarrow BN$ (20)

Upon reduction of 4-BrBN by $CO_2^{\bullet-}$, eq 17, the resulting 4-bromobenzonitrile radical anion (4-BrBN$^{\bullet-}$) is reported to decompose within 1 ns (i.e., k_f^{15} = 1 x 10^{10} s^{-1}) to form a neutral benzonitrile radical (BN$^{\bullet}$) and bromide (Br^{-}), eq 18.[55] BN$^{\bullet}$ is readily reduced by $CO_2^{\bullet-}$ to form the benzonitrile anion (BN^{-}), eq 19, which can be protonated by the solvent (DMF), supporting electrolyte (TBA^{+}), or residual H_2O, eq 20.[53, 55]

Figure 9 shows a comparison between experimental (solid) and simulated (dashed) voltammograms for solutions containing 0.9 mM DiMeFc, 5.5 mM $C_2O_4^{2-}$, and 0.0, 5.0, 10, and 40 mM 4-BrBN. Excellent agreement between experiment and simulation is obtained using the kinetic and thermodynamic parameters listed in Table 3. An expanded data set comparing experiments and simulations for eight different concentrations of 4-BrBN is shown in Figure S33. Note that the range of k_f^{15} values in Table 2 (10^6–10^{10} $M^{-1}s^{-1}$) is consistent with the more precise value given in Table 3, k_f^{15} = 1 x 10^8 $M^{-1}s^{-1}$.

Table 3. Simulation Parameters for the Oxidative Reduction of 4-BrBN[a]

Eq No.	Reaction	K_{eq}	k_f
15	$DiMeFc^{+} + CO_2^{\bullet-} \rightarrow DiMeFc + CO_2$	4.0 x 10^{43}	1 x 10^8 $M^{-1}s^{-1}$
17	$4\text{-}BrBN + CO_2^{\bullet-} \rightleftarrows 4\text{-}BrBN^{\bullet-} + CO_2$	3.7 x 10^4	4 x 10^6 $M^{-1}s^{-1}$
18	$4\text{-}BrBN^{\bullet-} \rightleftarrows BN^{\bullet} + Br^{-}$	3.2 x 10^3 M	1 x 10^{10} s^{-1}
19	$BN^{\bullet} + CO_2^{\bullet-} \rightarrow BN^{-} + CO_2$	4.9 x 10^{49}	1 x 10^{10} $M^{-1}s^{-1}$
20	$BN^{-} + H^{+} \rightarrow BN$	4.0 x 10^8	1 x 10^{10} $M^{-1}s^{-1}$

[a]Black: calculated from available thermodynamic data; blue: assumed values; red: literature values; green: determined from best fit of digital simulations to experimental CVs

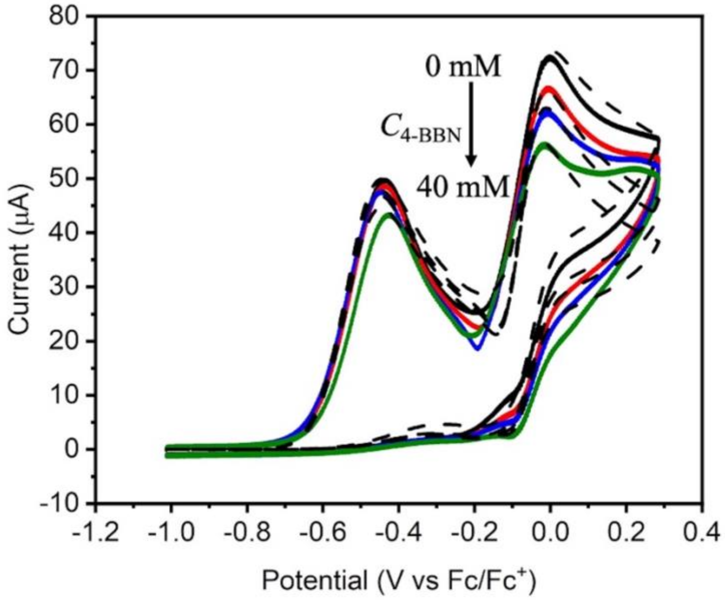

Figure 9. Experimental (solid lines) and simulated (dashed lines) CVs for solutions containing 0.9 mM DiMeFc, 5.5 mM CO_4^{2-}, and 0.0 (black), 5.0 (red), 10 (blue), and 40 (green) mM 4-bromobenzonitrile. All voltammograms were collected in an O_2-free DMF solution containing 0.1 M TBAP supporting electrolyte at ν = 100 mV/s. Details for the mechanism and parameters used for CV simulations can be found in the accompanying text as well as in Tables 3 and S4.

Eqs 19 and 20 are assumed to occur rapidly (i.e., $k_f^{19} = k_f^{20} = 1 \times 10^{10}\ M^{-1}s^{-1}$), with justifications provided in the Supporting Information. We note that the equilibrium constants for eqs 19 and 20 reported in Table 3 represent approximations due to a lack of thermochemical data. Specifically, $E^0(BN^\bullet/BN^-)$ is not available, so $E^0(C_6H_6^\bullet/C_6H_6^-)$ was used to compute K_{eq}^{19}, while the value for K_{eq}^{20} assumes H_2O as the proton source. Additional details for the approximation of both equilibrium constants are provided in the Supporting Information. Nonetheless, k_f^{15} and k_f^{17} remain as the sole fitting parameters for the simulations shown in Figure 9 since values for k_f^{13} and k_f^{14} were found from simulations in the absence of 4-BrBN, Figure 7. Parameter sensitivity analysis shown in Figures S34–S38 illustrate that the combination of $k_f^{15} = 1 \times 10^8\ M^{-1}s^{-1}$ and k_f^{17}

= 4 x 10^6 $M^{-1}s^{-1}$ gives the best fit of the digital simulation to the experimental CVs. For example, the simulated i_{pa} for DiMeFc$^+$-mediated $C_2O_4{}^{2-}$ oxidation no longer matches the experiment for any order-of-magnitude deviation of $k_f{}^{15}$ from 1 x 10^8 $M^{-1}s^{-1}$, Figure S36. Analogously, if, upon changing $k_f{}^{15}$ by one-order of magnitude, $k_f{}^{17}$ is altered to fit i_{pa} for DiMeFc$^+$-mediated $C_2O_4{}^{2-}$ oxidation, then the simulated i_{pa} for direct $C_2O_4{}^{2-}$ oxidation no longer agrees with the experiment, Figure S37. Concentration profiles, shown in Figure S39, exhibit the consumption of $CO_2{}^{\bullet-}$ to generate BN$^\bullet$.

These simulations provide an important design principle the oxidative reduction method: SET from $CO_2{}^{\bullet-}$ to the substrate must be sufficiently fast to outcompete SET from $CO_2{}^{\bullet-}$ to the oxidized form of the mediator. Note that this does not require that the rate constant for SET from $CO_2{}^{\bullet-}$ to the substrate is larger than the rate constant for SET from $CO_2{}^{\bullet-}$ to the oxidized form of the mediator. Rather, the rate constant for substrate reduction by $CO_2{}^{\bullet-}$ relative to the rate constant for reduction of the oxidized form of the mediator by $CO_2{}^{\bullet-}$ must be sufficiently large. Specifically, optimized values in this work find that the ratio $k_f{}^{17}/k_f{}^{15}$ = 4 x 10^{-2} is suitable for oxidative reduction to proceed. Alternatively, if $k_f{}^{17}$ = 1 x 10^5, as is the case for one of the simulations shown in Figure S34, then $k_f{}^{17}/k_f{}^{15}$ = 1 x 10^{-3} and 4-BrBN reduction is not observed. Further qualitative evidence of this can be seen by comparison of Figures 6B and C where debromination products are obtained in higher yield than dechlorination products, where SET from $CO_2{}^{\bullet-}$ to a C–Cl bond is expected to be slower than SET from $CO_2{}^{\bullet-}$ to a C–Br bond.

Conclusions

We have demonstrated that reductive hydrodehalogenation of electron-deficient aryl halides, a reaction that is typically carried out using very negative reducing conditions in dry solvents, can be carried out via mediated $C_2O_4^{2-}$ oxidation in mixed DMF/H_2O solutions at low potentials. Specifically, oxidation of DiMeFc at a carbon anode results in homogeneous $C_2O_4^{2-}$ oxidation, which leads to *in-situ* generation of a potent reductant, $CO_2^{\bullet-}$. We have shown that $CO_2^{\bullet-}$ produced by homogeneous $C_2O_4^{2-}$ oxidation is capable of reductively cleaving Ar–X (X = Br, Cl) bonds, enabling up to quantitative conversion yields for reductive hydrodehalogenation reactions. Cyclic voltammetry analysis indicates that the efficiency of the reaction can be tuned by additions of H_2O, a result confirmed by bulk electrolysis. Finite difference simulations suggest that the formation of $CO_2^{\bullet-}$ for use in the homogeneous reduction of Ar–X is enabled by mediating $C_2O_4^{2-}$ oxidation.

Use of the oxidative reduction method generally allows organic molecules to be reduced at an anode. As such, a sacrificial anode or oxidant is not necessary as the hydrogen evolution reaction can serve as the supporting half-reaction. In addition, the reduction of water and protons does not interfere with electroorganic reduction reactions occurring at an anode. We believe this method may provide a convenient platform for carrying out more complicated electroorganic reactions, such as reductive cross-coupling, where reaction intermediates are at risk of being over-reduced.

Associated Content

Supporting Information

The Supporting Information is available free of charge at (link).

Materials and methods, details of CV studies, CV control experiments, expanded CV data sets, details of bulk electrolysis, product isolation procedure, mass spectra, chromatograms, parameters used for digital simulation of cyclic voltammograms, and additional concentration profiles.

Author Information

Corresponding Author

Henry S. White – *Department of Chemistry, University of Utah, Salt Lake City, Utah 84112, United States*; orcid.org/ 0000-0002-5053-0996; Email: white@chemistry.utah.edu

Authors

Joshua A. Beeler – *Department of Chemistry, University of Utah, Salt Lake City, Utah 84112, United States*; orcid.org/0009-0001-9882-3173

Rune P. Walkingshaw – *Department of Chemistry, University of Utah, Salt Lake City, Utah 84112, United States*

Safiya A.S. Hamud – *Department of Chemistry, University of Utah, Salt Lake City, Utah 84112, United States*

Notes

The authors declare no competing financial interest.

Acknowledgements

This work was supported by the National Science Foundation Center for Synthetic Organic Electrochemistry (CHE-2002158). Mass spectra included in the report were collected at the University of Utah Optical Spectroscopy Lab and in the laboratory of Prof. Shelley D. Minteer. Chromatograms were collected in the laboratory of Prof. Shelley D. Minteer. J.A.B. acknowledges the Graduate Innovation Fellowship from the College of Science at the University of Utah.

References

(1) Yan, M.; Kawamata, Y.; Baran, P. S. Synthetic Organic Electrochemical Methods Since 2000: On the Verge of a Renaissance. *Chem. Rev.* **2017**, *117*, 13230–13319.

(2) Francke, R.; Little, R. D. Redox catalysis in organic electrosynthesis: basic principles and recent developments. *Chem. Soc. Rev.* **2014**, *43*, 2492–2521.

(3) Huang, B.; Sun, Z.; Sun, G. Recent progress in cathodic reduction-enabled organic electrosynthesis: Trends, challenges, and opportunities. *eScience* **2022**, *2*, 243–277.

(4) Carniero, S. N.; Laffoon, J. D.; Luo, L.; Sanford, M. S. Benchmarking Trisaminocyclopropeniums as Mediators for Anodic Oxidation Reactions. *J. Org. Chem.* **2024**, *89*, 6389–6394.

(5) Semmelhack, M. F.; Chou, C. S.; Cortes, D. A. Nitroxyl-Mediated Electrooxidation of Alcohols to Aldehydes and Ketones. *J. Am. Chem. Soc.* **1983**, *105*, 4492–4494.

(6) Platen, M.; Steckhan, E. Oxidative Deblocking of the 4-Methoxybenzyl Thioester Protecting Group: Application to the Directed Synthesis of Poly-cystinyl Peptides. *Liebigs Ann. Chem.* **1984**, *1984* (9), 1563–1576.

(7) Maki, T.; Iikawa, S.; Mogami, G.; Harasawa, H.; Matsumura, Y.; Onomura, O. Efficient Oxidation of 1,2-Diols into a-Hydroxyketones Catalyzed by Organotin Compounds. *Chem. Eur. J.* **2009**, *15*, 5364–5370.

(8) Kuhn, A. T. Kinetic Study of the Electrolytic Oxidation of Manganese(II) to Manganese(III) in Sulphuric Acid. *J. Chem. Soc. Faraday Trans. 1* **1983**, *79*, 417–430.

(9) Wagoner, E. R.; Hayes, J. L.; Karty, J. A.; Peters, D. G. Direct and nickel(I) salen-catalyzed reduction of 1,1,2-trichloro-1,2,2-trifluoroethane (CFC-113) in dimethylformamide. *J. Electroanal. Chem.* **2012**, *676*, 6–12.

(10) Du, P.; Mubarak, M. S.; Karty, J. A.; Peters, D. G. Electrosynthesis of 4-Methylcoumarin via Cobalt(I)-Catalyzed Reduction of 2-Acetylphenyl 2-Chloroacetate or 2-Acetylphenyl 2,2-Dichloroacetate. *J. Electrochem. Soc.* **2007**, *154* (12), F231–F237.

(11) Fuchigami, T.; Kasuga, M.; Konno, A. Electro-organic chemistry of fullerenes. Part 1. Indirect cathodic reduction of *vic*-dihalides and perflouroalkyl halides using C_{60} as mediator. Cyclic voltammetric study and preparative-scale electrolysis. *J. Electroanal. Chem.* **1996**, *411*, 115–119.

(12) Boujlel, K.; Simonet, J. Cathodic cleavage of carbon-oxygen bonds (V). direct and indirect electrochemical reduction of epoxides. *Electrochim. Acta* **1979**, *24* (5), 481–487.

(13) Park, S. H.; Ju, M.; Ressler, A. J.; Shim, J.; Kim, H.; Lin, S. Reductive Electrosynthesis: A New Dawn. *Aldrichimica ACTA* **2021**, *54* (17–27).

(14) Hu, P.; Peters, B. K.; Malapit, C. A.; C., V. J.; Wang, P.; Li, J.; Mele, L.; Echeverria, P.-G.; Minteer, S. D.; Baran, P. S. Electroreductive Olefin–Ketone Coupling. *J. Am. Chem. Soc.* **2020**, *142*, 20979–20986.

(15) Yang, D.-T.; Zhu, M.; Schiffer, Z. J.; Williams, K.; Song, X.; Liu, X.; Manthiram, K. Direct Electrochemical Carboxylation of Benzylic C–N Bonds with Carbon Dioxide. *ACS Catal.* **2019**, *9*, 4699–4705.

(16) Xiao, W.; Zhang, J.; Wu, J. Recent Advances in Reactions Involving Carbon Dioxide Radical Anion. *ACS Catal.* **2023**, *13*, 15991–16011.

(17) Hendy, C. M.; Smith, G. C.; Xu, Z.; Lian, T.; Jui, N. T. Radical Chain Reduction via Carbon Dioxide Radical Anion ($CO_2^{\bullet-}$). *J. Am. Chem. Soc.* **2021**, *143*, 8987–8992.

(18) Chmiel, A. F.; Williams, O. P.; Chernowsky, C. P.; Yeung, C. S.; Wickens, Z. K. Non-innocent Radical Ion Intermediates in Photoredox Catalysis: Parrallel Reduction Modes Enable Coupling of Diverse Aryl Chlorides. *J. Am. Chem. Soc.* **2021**, *143*, 10882–10889.

(19) Wang, S.-D.; Yang, B.; Zhang, H.; Qu, J.-P.; Kang, Y.-B. Reductive Cleavage of C–X or N–S Bonds Catalyzed by Super Organoreductant CBZ6. *Org. Lett.* **2023**, *25*, 816–820.

(20) Wang, H.; Gao, Y.; Zhou, C.; Li, G. Visible-Light-Driven Reductive Carboarylation of Styrenes with CO_2 and Aryl Halides. *J. Am. Chem. Soc.* **2020**, *142*, 8122–8129.

(21) Hang, W.; Li, D.; Zou, S.; Xi, C. Visible-Light-Driven Reductive Carboxylation of Benzyl Bromides with Carbon Dioxide Using Formate as Terminal Reductant. *J. Org. Chem.* **2023**, *88*, 5007–5014.

(22) Zhou, C.; Wang, X.; Yang, L.; Fu, L.; Li, G. Visible-light-driven regioselective carbocarboxylation of 1,3-dienes with organic halides and CO_2. *Green Chem.* **2022**, *24*, 6100–6107.

(23) Hou, J.; Hua, L.-L.; Huang, Y.; Zhan, L.-W.; Li, B.-D. Visible-Light-Promoted Catalyst-Free Oxyarylation and Hydroarylation of Alkenes with Carbon Dioxide Radical Anion. *Chem.—Asian J.* **2022**, *18*, e202201092.

(24) Huang, Y.; Zhang, Q.; Hua, L.-L.; Zhan, L.-W.; Hou, J.; Li, B.-D. A versatile catalyst-free redox system mediated by carbon dioxide radical and dimsyl anions. *Cell Rep. Phys. Sci.* **2022**, *3*, 100994.

(25) Seo, H.; Liu, A.; Jamison, T. F. Direct ß-Selective Hydrocarboxylation of Styrenes with CO_2 Enabled by Continuous Flow Photoredox Catalysis. *J. Am. Chem. Soc.* **2017**, *139*, 13969–13972.

(26) Huang, H.; Ye, J.-H.; Zhu, L.; Ran, C.-K.; Miao, M.; Wang, W.; Chen, H.; Zhou, W.-J.; Lan, Y.; Yu, B.; Yu, D.-H. Visible-Light-Driven Anti-Markovnikov Hydrocarboxylation of Acrylates and Styrenes with CO_2. *CCS Chem.* **2020**, *2*, 1746–1756.

(27) Ju, T.; Zhou, Y.-Q.; Cao, K.-G.; Fu, Q.; Ye, J.-H.; Sun, G.-Q.; Liu, X.-F.; Chen, L.; Liao, L.-L.; Yu, D.-G. Dicarboxylation of alkenes, allenes, and (hetero)arenes with CO_2 via visible-light photoredox catalysis. *Nat. Catal.* **2021**, *4*, 304–311.

(28) Alektiar, S. N.; Han, J.; Dang, Y.; Rubel, C. Z.; Wickens, Z. K. Radical Hydrocarboxylation of Unactivated Alkenes via Photocatalytic Formate Activation. *J. Am. Chem. Soc.* **2023**, *145*, 10991–10997.

(29) Song, L.; Wang, W.; Yue, J.-P.; Jiang, Y.-X.; Wei, M.-K.; Zhang, H.-P.; Yan, S.-S.; Liao, L.-L.; Yu, D.-G. Visible-light photocatalytic di- and hydro-carboxylation of unactivated alkenes with CO_2. *Nat. Catal.* **2022**, *5*, 832–838.

(30) Alektiar, S. N.; Wickens, Z. K. Photoinduced Hydrocarboxylation via Thiol-Catalyzed Delivery of Formate Across Activated Alkenes. *J. Am. Chem. Soc.* **2021**, *143*, 13022–13028.

(31) Xiao, H.-Z.; Yu, B.; Yan, S.-S.; Zhang, W.; Li, X.-X.; Bao, Y.; Luo, S.-P.; Ye, J.-H.; Yu, D.-G. Photocatalytic 1,3-dicarboxylation of unactivated alkenes with CO_2. *Chin. J. Catal.* **2023**, *50*, 222–228.

(32) Koppenol, W. H.; Rush, J. D. Reduction Potential of the $CO_2/CO_2^{\bullet-}$ Couple. A Comparison with Other C_1 Radicals. *J. Phys. Chem.* **1987**, *91*, 4429–4430.

(33) Alkayal, A.; Tabas, V.; Montanaro, S.; Wright, I. A.; Malkov, A., V.; Buckley, B. R. Harnessing Applied Potential: Selective ß-Hydrocarboxylation of Substituted Olefins. *J. Am. Chem. Soc.* **2020**, *142*, 1780–1785.

(34) Kim, Y.; Park, G. D.; Balamurugan, M.; Seo, J.; Min, B. K.; Nam, K. T. Electrochemical ß-Selective Hydrocarboxylation of Styrene Using CO_2 and Water. *Adv. Sci.* **2020**, *7*, 1900137.

(35) Sheta, A. M.; Alkayal, A.; Mashaly, M. A.; Said, S. B.; Elmorsy, S. S.; Malkov, A., V.; Buckley, B. R. Selective Electrosynthetic Hydrocarboxylation of α,ß-Unsaturated Esters with Carbon Dioxide. *Angew. Chem. Int. Ed.* **2021**, *60*, 21832–21837.

(36) You, Y.; Kanna, W.; Takano, H.; Hayashi, H.; Maeda, S.; Mita, T. Electrochemical Dearomative Dicarboxylation of Heterocycles with Highly Negative Reduction Potentials. *J. Am. Chem. Soc.* **2022**, *144*, 3685–3695.

(37) Zhang, W.; Liao, L.-L.; Li, L.; Liu, Y.; Dai, L.-F.; Sun, G.-Q.; Ran, C.-K.; Ye, J.-H.; Lan, Y.; Yu, D.-G. Electroreductive Dicarboxylation of Unactivated Skipped Dienes with CO_2. *Angew. Chem. Int. Ed.* **2023**, *62*, e202301892.

(38) Zhao, Z.; Liu, Y.; Wang, S.; Tang, S.; Ma, D.; Zhu, Z.; Guo, C.; Qiu, Y. Site-Selective Electrochemical C–H Carboxylation of Arenes with CO_2. *Angew. Chem. Int. Ed.* **2023**, *62*, e202214710.

(39) Zhang, K.; Ren, B.-H.; Lie, X.-F.; Wang, L.-L.; Zhang, M.; Ren, W.-M.; Lu, X.-B.; Zhang, W.-Z. Direct and Selective Electrocarboxylation of Styrene Oxides with CO_2 for Accessing ß-Hydroxy Acids. *Angew. Chem. Int. Ed.* **2022**, *61*, e202207660.

(40) Wang, Y.; Tang, S.; Yang, G.; Wang, S.; Ma, D.; Qiu, Y. Electrocarboxylation of Aryl Epoxides with CO_2 for the Facile and Selective Syntehsis of ß-Hydroxy Acids. *Angew. Chem. Int. Ed.* **2022**, *61*, e202207746.

(41) Chang, M.-M.; Saji, T.; Bard, A. J. Electrogenerated Chemiluminescence. 30. Electrochemical Oxidation of Oxalate Ion in the Presence of Luminescers in Acetonitrile Solutions. *J. Am. Chem. Soc.* **1977**, *99* (17), 5399–5403.

(42) Rubenstein, I.; Bard, A. J. Electrogenerated Chemiluminescence. 37. Aqueous Ecl Systems Based on $Ru(2,2'\text{-bipyridine})_3^{2+}$ and Oxalate or Organic Acids. *J. Am. Chem. Soc.* **1981**, *103*, 512–516.

(43) Rubenstein, I.; Martin, C. R.; Bard, A. J. Electrogenerated Chemiluminescent Determination of Oxalate. *Anal. Chem.* **1983**, *55*, 1580–1582.

(44) Ege, D.; Becker, W. G.; Bard, A. J. Electrogenerated Chemiluminescent Determination of $Ru(bpy)_3^{2+}$ at Low Levels. *Anal. Chem.* **1984**, *56*, 2413–2417.

(45) Kanoufi, F.; Bard, A. J. Electrogenerated Chemiluminescence. 65. An Investigation of the Oxidation of Oxalate by Tris(polypyridine) Ruthenium Complexes and the Effect of the Electrochemical Steps on the Emission Intensity. *J. Phys. Chem. B* **1999**, *103*, 10469–10480.

(46) Kanoufi, F.; Cannes, C.; Zu, Y.; Bard, A. J. Scanning Electrochemical Microscopy. 43. Investigation of the Oxalate Oxidation and Electrogenerated Chemiluminescence across the Liquid–Liquid Interface. *J. Phys. Chem. B* **2001**, *105*, 8951–8962.

(47) Kai, T.; Zhou, M.; Johnson, S.; Ahn, H. S.; Bard, A. J. Direct Observation of $C_2O_4^{\cdot -}$ and $CO_2^{\cdot -}$ by Oxidation of Oxalate within Nanogap of Scanning Electrochemical Microscope. *J. Am. Chem. Soc.* **2018**, *140*, 16178–16183.

(48) Isse, A. A.; Gennaro, A.; Maran, F. Mechanism of the Dissociative Electro-oxidation of Oxalate in Aprotic Solvents. *Acta Chem. Scand.* **1999**, *53*, 1013–1022.

(49) Beeler, J. A.; Tanwar, M.; Neurock, M.; White, H. S. Solvent-Dependent Mechanism of Electrochemical Oxalate Oxidation. *In Preparation*.

(50) Bard, A. J.; Faulkner, L. R.; White, H. S. *Electrochemical Methods: Fundamentals and Applications*; 2022.

(51) Fogg, P. G. *Carbon Dioxide in non-aqueous solvents at pressures less than 200 kPa*; Elsevier, 2017.

(52) Hosseini, S.; Janusz, J. N.; Tanwar, M.; Pendergast, A. D.; Neurock, M.; White, H. S. Oxidation by Reduction: Efficient and Selective Oxidation of Alcohols by the Electrocatalytic Reduction of Peroxydisulfate. *J. Am. Chem. Soc.* **2022**, *144*, 21103–21115.

(53) Bartak, D. E.; Houser, K. J.; Rudy, B. C.; Hawley, M. D. Electrochemical Studies of the Formation and Decomposition of Halogenated Benzonitrile Anion Radicals. *J. Am. Chem. Soc.* **1972**, *94*, 7526–7530.

(54) Clegg, A. D.; Rees, N. V.; Klymenko, O. V.; Coles, B. A.; Compton, R. G. Marcus theory of outer-sphere heteregeneous electron trasnfer reactions: High precision steady-state measurements of the standard electrochemical rate constant for ferrocene derivatives in alkyl cyanide solvents. *J. Electroanal. Chem.* **2005**, *580*, 78–86.

(55) M'Halla, F.; Pinson, J.; Savéant, J. M. The Solvent as H-Atom Donor in Organic Electrochemical Reactions. Reduction of Aromatic Halides. *J. Am. Chem. Soc.* **1980**, *102*, 4120–4127.